HHS Public Access

Author manuscript

ACS Biomater Sci Eng. Author manuscript; available in PMC 2016 December 14.

Published in final edited form as:

ACS Biomater Sci Eng. 2016 December 12; 2(12): 2217–2230. doi:10.1021/acsbiomaterials.6b00419.

Tuning Hydrogel Properties to Promote the Assembly of Salivary Gland Spheroids in 3D

Tugba Ozdemir[1,$], **Eric W. Fowler**[1,$], **Shuang Liu**[1], **Daniel A. Harrington**[2], **Robert L. Witt**[3,4], **Mary C Farach-Carson**[2,3,5,#], **Swati Pradhan-Bhatt**[3,4,6,*], and **Xinqiao Jia**[1,3,6,*]

[1]Department of Materials Science and Engineering, University of Delaware, 210 South College Ave., Newark, DE 19716, USA

[2]Department of BioSciences, Rice University, 6100 Main St., Houston, TX 77005, USA

[3]Department of Biological Sciences, University of Delaware, 210 South College Ave., Newark, DE, 19716, USA

[4]Helen F. Graham Cancer Center and Research Institute, Christiana Care Health Systems, 4701 Ogletown Stanton Rd., Newark, DE, 19713, USA

[5]Department of Bioengineering, Rice University, 6100 Main St., Houston, TX 77005, USA

[6]Department of Biomedical Engineering, University of Delaware, 210 South College Ave., Newark, DE 19716, USA

Abstract

Current treatments for chronic xerostomia, or “dry mouth”, do not offer long-term therapeutic benefits for head and neck cancer survivors previously treated with curative radiation. Towards the goal of creating tissue-engineered constructs for the restoration of salivary gland functions, we developed new hyaluronic acid (HA)-based hydrogels using thiolated HA (HA-SH) and acrylated HA (HA-AES) with a significant molecular weight mismatch. Four hydrogel formulations with varying HA concentration, (1–2.4 wt%) and thiol/acrylate ratios (2/1 to 36/1) and elastic moduli (G’: 35 to 1897 Pa, 2 h post-mixing) were investigated. In our system, thiol/acrylate reaction was initiated rapidly upon mixing of HA-SH/HA-AES to establish thioether crosslinks with neighboring ester groups, and spontaneous sulfhydryl oxidation occurred slowly over several days to install a secondary network. The concurrent reactions cooperatively create a cell-permissive network to allow for cell expansion and aggregation. Multicellular spheroids formed readily from a robust ductal epithelial cell line (Madin-Darby Canine Kidney, MDCK cells) in all hydrogel formulations investigated. Primary salivary human stem/progenitor cells (hS/PCs), on the other hand, are sensitive to the synthetic extracellular environment, and organized acini-like structures

[*]To whom correspondence should be addressed: Swati Pradhan-Bhatt, Phone: 302-623-4649, Fax: 302-623-4314, swati@udel.edu, Xinqiao Jia, Phone: 302-831-6553, Fax: 302-831-4545, xjia@udel.edu.

[$]These authors contributed equally to this work.

[#]Current affiliation: The University of Texas Health Science Center at Houston, School of Dentistry, Department of Diagnostic and Biomedical Sciences, 1941 East Road, Houston TX 77054, USA

Supporting information: Synthesis and characterization of hydrogel precursors, antibody information, flow cytometry characterization of cell surface CD44, fluorescent staining of cell surface thiol, 6-h in situ rheology of DRC18, appearance of DRC constructs after 27 days of culture, immunostaining for K5 and K14 on hS/PC spheroids grown in DRC2 and DRC4, F-actin staining of hS/PCs grown in HA-SH/HA-AM and 3D reconstructed confocal image of hS/PC spheroid.

with an average diameter of 50 μm were obtained only in gels with G' ≤ 216 Pa and a thiol/acrylate ratio ≥18. The spheroid size and size distribution were dependent on the HA content in the hydrogel. Cells in hS/PC spheroids formed tight junctions (occludin), remained viable and proliferative, secreted structural proteins (collagen IV and laminin) found in the basement membrane and maintained key stem/progenitor markers. We conclude that incorporation of time-dependent, dynamic features into a covalently crosslinked HA network produces an adaptable hydrogel framework that promotes hS/PC assembly and supports early aspects of salivary morphogenesis, key to reconstitution of a fully functional implantable salivary gland.

Graphical abstract

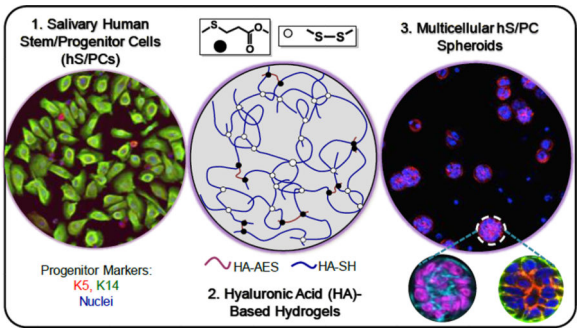

Keywords

Xerostomia; Salivary Human Stem/Progenitor Cells; Hyaluronic Acid-Based Hydrogels; Thiol/Acrylate Ratio; Elastic Modulus; Permissive Network

1. Introduction

Saliva is an aqueous mixture of various proteins and electrolytes produced by salivary cells to maintain oral health. Radiation therapy for treatment of head and neck cancers can result in acinar cell loss, periductal fibrosis and destruction of the capillary structures,[1] giving rise to xerostomia, or "dry mouth", a devastating syndrome affecting an estimated 62,000 head and neck cancer patients every year in the US alone.[2] Without the protective saliva, patients suffer from severe oral dryness, have difficulty speaking, swallowing, which can develop into dental caries and periodontal diseases. Current treatments for xerostomia only temporarily mitigate symptoms, but do not provide long-term therapeutic benefits.[3] Tissue engineering offers a potentially permanent clinical solution for the restoration of salivary function. Our autologous restoration paradigm relies on the *ex vivo* assembly of secretory and implantable neotissues using biomimetic and cell-instructive matrices that can guide the differentiation/assembly of adult stem/progenitor cells isolated from patients prior to radiation therapy.

Salivary gland tissue engineering is particularly challenging, as the tissue itself is a complex physiological system and requires coordinated actions of multiple cell types, including acinar, myoepithelial and ductal cells.[4–5] While a large body of literature describes the 3D culture of salivary gland cells in reconstituted gels from natural protein extracts that are not

human compatible,[6] very few studies are dedicated to the establishment of synthetic matrices with tunable materials properties for the assembly of complex salivary gland structures. Synthetic or semi-synthetic hydrogels utilized for salivary gland tissue engineering purposes are based largely on poly(ethylene glycol) (PEG) and/or hyaluronic acid (HA). One report of primary mouse submandibular gland cells, cultured within covalently crosslinked PEG gels, describes viability and phenotype retention for pre-aggregated cells encapsulated under specific crosslinking chemistries.[7] Stably crosslinked HA gels that effectively promoted the formation of prostate cancer spheroids[8–11] failed to promote the formation of salivary spheroids from individually-encapsulated salivary gland epithelial cells. Although covalently crosslinked HA/PEG gels allowed for the growth of lobular structures two weeks after 3D cell encapsulation,[12–13] the underlying mechanism has not been elucidated and thorough integration of implanted cell-gel constructs with host tissues is challenging owing to their relatively low *in vivo* stability.

These earlier investigations underscore the importance of careful examination and fine tuning of crosslinking chemistry as well as hydrogel structure and properties to enable the 3D assembly of salivary epithelial cells. Unfortunately, to this date, synthetic or semi-synthetic hydrogels that facilitate the rapid assembly of multicellular spheroids from dispersed single cells, stimulate differentiation towards the desired lineage, and facilitate long term tissue integration have not yet been developed. Fundamentally, encapsulating epithelial cells in a stably crosslinked “covalent cage” with nanosized pores does not give rise to organized 3D assemblies because cells cannot easily proliferate and/or migrate towards each other in such networks. To promote spheroid formation, and ultimately more complex structures, from dispersed single cells, a more permissive network structure must be created. This can be achieved by tuning crosslinker length, linker chemistry, network connectivity and degree of crosslinking. Because HA is involved in diverse biological processes, including tissue morphogenesis and wound healing,[14] a hydrogel system that is purely HA-based is desirable for salivary gland regeneration purposes. Further improvement of gel stability and facile manipulation of gel properties allow an in-depth analysis of the structure-function relationship, contributing to the successful engineering of functional implants.

Herein, we describe a new type of HA hydrogel containing hydrolytically degradable moieties and adaptable disulfide linkages (Scheme 1) for *in vitro* assembly of salivary spheroids structures using expanded cultures of primary salivary human stem/progenitor cells (hS/PCs).[13] These hydrogels were prepared using thiolated HA (HA-SH) and acrylated HA (synthesized via reaction with mono-2-(acryloyloxy)ethyl succinate, HA-AES) with a molecular weight and stoichiometry mismatch. We altered the hydrogel properties by varying HA concentration and thiol/acrylate ratio. In our system, both thiol/acrylate Michael reaction and sulfhydryl oxidation contribute to the rapid formation of a loose network for 3D encapsulation of dispersed epithelial cells. Additional S-S bonds that form slowly over time not only further stabilize the network but also provide a permissive environment for cell assembly. The resultant hydrogels were characterized in terms of their compositional, mechanical, swelling and degradation properties. We first validated our hydrogel design using a well-established polarizing epithelial cell line, MDCK cells. Subsequent 3D culture of hS/PCs resulted in the formation of well-organized, stable spherical structures analogous

to the acini found in the native tissue. Finally, we analyzed the cellular organization of spheroid structures by evaluating the localization of cell-cell adhesion proteins and the expression of progenitor markers necessary for long term tissue morphogenesis.

2. Materials and Methods

2.1. Materials

Low (5 kDa) and high (500 kDa) molecular weight HA were obtained from Lifecore Biomedical (Chaska, MN) and Genzyme Corporation (Cambridge, MA), respectively. Succinic anhydride, 1-ethly-3-(3-(dimethlyamino)propyl)carbodiimide (EDC), dithiothreitol (DTT), 2-hydroxyethyl acrylate, 1-methylimidazole, di-*tert*-butyl dicarbonate (Boc_2O), 4-dimethylaminopyridine (DMAP), tetrabutylammonium hydroxide (TBA-OH), dimethyl sulfoxide (DMSO), 5-(3-carboxy-4-nitrophenyl)disulfanyl-2-nitrobenzoic acid (DTNB), sodium acetate, phosphate buffered saline (PBS, 1×), bovine testicular hyaluronidase (HAase, 30,000 U/mg), and trypsin soybean inhibitor were obtained from Sigma-Aldrich (Milwaukee, WI). Deionized water (DI) was sourced from a NANOpure Diamond water purification system (Thermo Scientific, Barnstead, NH). HepatoSTIM™ medium was purchased from Corning Life Sciences (Corning, NY). Fungizone® and PicoGreen dsDNA assay kit were purchased from Thermo Fisher (Carlsbad, CA). Dulbecco's Modified Eagle Medium (DMEM)/Nutrient Mixture F-12 and TrypLE™ Express were obtained from Life Technologies (Carlsbad, CA). Fetal bovine serum (FBS, 10%) was purchased from Denville Scientific (Metuchen, NJ). Information on primary antibodies used for immunofluorescence is summarized in Table S1. Alexa Fluor 488 or Alexa Fluor 647-labeled secondary antibodies (Molecular Probes) against mouse or rabbit IgG (produced in goat) were used. F-Actin and nuclei were stained with Alexa Fluor 568 Phalloidin (Molecular Probes) and DAPI (Pierce), respectively. Fluorescein isothiocyanate (FITC)-labeled mouse anti-human Ki67 were purchased from Molecular Probes (Carlsbad, CA). For flow cytometry, allophycocyanin (APC)-conjugated mouse anti-human CD44 and IgG antibodies were obtained from BD Pharmingen (San Diego, CA).

2.2. Synthesis of HA-SH and HA-AES

Acrylate groups were conjugated to HA via an esterification reaction with mono-2-(acryloyloxy)ethyl succinate (AES, Scheme S1, Figure S1A) in an organic medium using a low molecular weight HA (5 kDa, tetrabutylammonium salt), as described in the Supporting Information. The product, HA-AES, was obtained after precipitation, ion exchange and dialysis at a 45% yield with a 50% AES incorporation based on ^1H NMR (Figure S1B). Sulfhydryl groups were incorporated in HA (500 kDa) via an EDC-mediated coupling reaction with 3,3'-dithiobis-propanoic dihydrazide (DTP) in an aqueous media at pH 4.75, followed by reduction with DTT, according to reported methods.[9, 15] The solid product, HA-SH, was obtained at 80% yield, with a 40% thiol incorporation based on ^1H NMR (Figure S1C). For cell culture purposes, the dialyzed solutions were sterilized using a 0.22 μm filter prior to lyophilization. The chemically modified HA products were stored at −20 °C prior to use.

2.3. Hydrogel synthesis and characterization

2.3.1. Hydrogel synthesis—HA-SH was dissolved in PBS at concentrations of 10 or 20 mg/mL and the solution pH was adjusted to 7.4 using concentrated NaOH (1.0 M). HA-AES was separately dissolved in PBS at pH 7.4 to afford 10 or 100 mg/mL solutions. HA-SH and HA-AES solutions were thoroughly mixed at 20/1 (v/v), and the resultant hydrogels were designated as DRCx, with x indicating the molar excess of thiols relative to the acrylates in the final gel formulation (Table 1). The mixture was aliquoted to cell culture inserts (diameter: 12 mm, pore size: 0.4 μm) and incubated at 37 °C for 2 h to obtain fully crosslinked hydrogel discs.

2.3.2. High resolution magic angle spinning (HR-MAS) ^{1}H NMR—The hydrogel components were dissolved at their respective concentrations in D_2O. The pH of HA-SH solution was adjusted to 7.4 using 1.0 M NaOD in D_2O. Immediately after the addition of the HA-AES solution, the mixture was loaded into a Bruker KeL-F insert. Measurements were performed using a 4 mm rotor at 6,000 Hz on a Bruker AV600 using a high resolution magic angle spinning probe. The acrylate concentration (mM) in the hydrogel was determined by monitoring the vinyl protons at 6.33, 6.10, and 5.89 ppm, assuming no reaction occurred at time zero.

2.3.3. Oscillatory rheology—The viscoelastic properties of HA gels were analyzed using a TA instrument DHR-3 rheometer with a 12 mm stainless steel geometry and 500 μm gap size at 37 °C. Time sweep was performed with 0.1% strain at 1 Hz. Promptly after mixing, the precursor mixture was loaded on a plate/plate geometry, and mineral oil was applied around the geometry to prevent evaporation. After two hours, a frequency sweep from 0.1 to 10 Hz was performed at 0.1% strain. Measurements were conducted in triplicate and the average storage (G') and loss (G") moduli are reported.

2.3.4. Swelling ratio and hydrolytic degradation—Hydrogel swelling and degradation were analyzed gravimetrically and colorimetrically. Hydrogel degradation was evaluated based on the HA release from the gel network over time. Specifically, hydrogel precursors (90 μL) were thoroughly mixed, aliquoted to cell culture inserts and incubated at 37 °C for 30 min. PBS (800 μL) was subsequently added to each well and the gels were incubated at 37 °C for up to 28 days. At a predetermined time (1, 4, 7, 10, 14, 21 and 28 days), the conditioned buffer was removed, the wet gel mass was recorded, and fresh PBS was added. The swelling ratio was calculated from the initial HA mass in feed and the measured wet weight. The PBS solution extracted from each time point was subjected to carbazole assay to determine the amount of HA released into the supernatant.[16] The remaining gel mass, calculated by normalizing HA found in the supernatant to the initial HA content in feed, was used as an indication of time-dependent hydrogel degradation. All measurements were performed in triplicate.

2.3.5. Thiol consumption—The time-dependent consumption of thiols in each hydrogel formulation was quantified via modified Ellman's assay. Briefly, 5 μL of the hydrogel mixture was incubated for 2 h at 37 °C. The gel disk was then mixed with 250 μL of Ellman's Reagent (50 mM sodium acetate and 10 mM DTNB in DI water) and 100 μL of

PBS. Samples were rotated at 1,400 RPM on an Eppendorf thermomixer (Hamburg, Germany) at 50 °C for 10 min. Subsequently, 645 μL of DI water was added and the mixture was vortexed at 50 °C for 5 min. The solution absorbance was recorded at 405 nm on a Wallac 1420 Victor2™ plate reader (Perkin Elmer, Rodgau, Germany). The time-dependent thiol consumption was calculated by comparison to a cysteine standard. For time points beyond 2 h, the hydrogel was allowed to swell with 40 μL of PBS and at the time of analysis the PBS volume was made up to 100 μL.

2.4. Cell maintenance

Madin-Darby Canine Kidney (MDCK) NBL-2 cells were obtained from ATCC (Manassas, VA) and were maintained in CellTreat (Shirley, MA) tissue culture flasks (75 cm^2) at 37 °C in 5% (v/v) CO_2 in an Eagle's minimal essential medium with 100 IU/mL penicillin/streptomycin and 10% FBS. The medium was changed every 2 days and cells were routinely passaged using 0.25% Trypsin/0.02%EDTA.

Primary hS/PCs were isolated as previously reported[13] from parotid tissue collected from consented patients, both male and female, undergoing surgery under protocols approved by both the Christiana Care Health Systems and the University of Delaware IRBs. After procurement, the tissue was disinfected with 1% (v/v) betadine solution in cold DMEM/F-12, minced into a slurry and suspended in HepatoSTIM™ medium supplemented with 100 IU/mL penicillin-streptomycin, 1% (v/v) Fungizone® and epidermal growth factor (EGF, 10 ng/ml). On reaching 70–80% confluence, hS/PCs were trypsinized using 0.05% (w/v) trypsin-EDTA for 5 min before an equal volume of 1 mg/mL trypsin soybean inhibitor was added. Cells were re-plated at a dilution of 1:4. Cells in passage 6–10 were used for all experiments.

2.5. Cell encapsulation

Prior to encapsulation, cells were trypsinized, dispersed and counted using trypan blue. Cells then were re-suspended in HA-SH (pH ~7.4) at a concentration of 0.25×10^6 cells/mL for MDCK cells and 1×10^6 cells/mL for hS/PCs. Upon addition of the HA-AES stock solution, 150 μL of the gelling liquid was thoroughly mixed and aliquoted to 12 mm cell culture inserts (Millipore) placed in 24 well plates. Gelation was allowed to proceed for 30 min at 37 °C before the appropriate cell culture media (500 μL) was added outside the inserts. The constructs were incubated for another 25 min at 37 °C before an additional 300 μL of media was added to the insert directly on top of the construct to complete the encapsulation process.

2.6. Biological characterization

2.6.1. Cell viability—At designated time points (day 1, 14 and 28 for hS/PC cultures and day 7 for MDCK cultures), the cell/gel constructs were recovered from the cell culture inserts and transferred into a glass bottom Lab-Tek multiwell chamber slide (Thermo Fisher) and were briefly washed with warm PBS. For live/dead staining, SYTO-13 and propidium iodide (PI) were diluted at 1:1000 and 1:2000 (v/v) respectively in warm PBS. Three hundred microliters of the staining mixture was added to the 3D constructs, and the samples were incubated at 37 °C for 30 min. Constructs were subsequently washed with warm PBS

(3 times) before being imaged with a Zeiss LSM 880 high speed multiphoton confocal microscope (Carl Zeiss, Maple Grove, MN). Each image represents a maximum intensity projection of 200 μm thick z-stacks taken from random locations in the hydrogels.

2.6.2. Cell Proliferation—On day 28, the hS/PC constructs were treated with HAase (10 kU/mL) at 37 °C for 4 h. Cells released from the matrices were collected by centrifugation at 5,000 RPM for 5 min. The cell pellets were then treated with papain digestion buffer (5 mM L-cysteine, 5 mM EDTA, 125 μg/mL papain, pH 6.4) at 60 °C for 16 h. The total DNA in the supernatant was quantified using PicoGreen dsDNA assay following manufacturer's protocol.

2.6.3. Immunofluorescence—Upon completion of 3D cultures, cell/gel constructs were transferred to a glass bottom chamber slide, thoroughly washed with PBS, and fixed with 4% paraformaldehyde (4%, v/v in PBS) for 30 min. Following a thorough wash after fixation, samples were incubated in a Permeabilization buffer (3% bovine serum albumin, 0.2% Triton-X 100 in PBS) overnight at 4 °C. Subsequently, a primary antibody (Table S1) diluted in the Permeabilization buffer was added and samples were incubated overnight at 4 °C. After a thorough PBS (3 times) wash, a secondary antibody solution containing the desired secondary antibody (1:200 dilution), phalloidin (1:250) and DAPI (1:1000) in Permeabilization buffer was introduced and the constructs were incubated at room temperature for 2 h. Finally, constructs were washed again with PBS (6 times) and imaged using a Zeiss LSM 880 high speed multiphoton confocal microscope.

2.6.4. Spheroid Growth Analysis—The size and size distribution of the hS/PC spheroids grown in HA hydrogels were quantified using ImageJ software (NIH, Bethesda, MD) based on 5 different images of fluorescently stained specimens (imaged as above, and deconvolved from 500 μm sections using Zeiss ZEN Software's Maximum Intensity Projection function) for each gel combination. The spheroid size distribution was created using a histogram plot with a 5 μm bin for the spheroid diameters measured. The resulting histogram was fitted with a Gaussian distribution using OriginPro Software.

2.7. Statistical analysis

All quantitative measurements were performed in triplicate. Statistical significance was evaluated using one-way ANOVA followed by Tukey-Kramer test for multiple comparisons. A p value of <0.05 was considered to be statistically significant.

3. Results

3.1. Hydrogel synthesis and characterization

Acrylated HA (HA-AES) was synthesized via the esterification reaction of AES with low molecular weight HA (5 kDa) under anhydrous organic conditions using BOC_2O/DMAP as an acyl-transfer agent (Supporting information). The product, HA-AES, had an average 50% functionalization based on ^{1}H-NMR (Figure S1B), and the reactive acrylate is coupled to the HA backbone through three ester linkages that are susceptible to hydrolysis. Separately, sulfhydryl groups were introduced to high molecular weight HA (500 kDa) via a

carbodiimide-mediated coupling reaction between HA and DTP. Subsequent reduction of the disulfide bond in the conjugate afforded HA-SH with an estimated thiolation degree of 40% determined from ^{1}H-NMR (Figure S1C).

Hydrogels were prepared by mixing HA-SH and HA-AES at a thiol/acrylate ratio varying from 2 to 36 (DRCx, Table 1). The kinetics of thiol/acrylate crosslinking was conveniently monitored by HR-MAS ^{1}H-NMR, following the disappearance of the vinyl protons between 5.89 and 6.33 ppm (Figure 1). For the DRC2 gels that have the highest acrylate concentration, although a semi-solid gel is formed 30 min after the precursors were mixed, the Michael addition reaction continues over the course of 90 min, at which point, signals from the vinyl protons were not detectable by HR-MAS ^{1}H NMR. No vinyl protons were detectable for the other gel formulations (DRC4, 18 and 36) even after immediate loading of each mixture into the MAS rotor; this is in agreement with an expected increase in the speed of acrylate consumption in those formulations that had a higher thiol/acrylate ratio

Oscillatory rheology (Figure 2) was subsequently performed on various HA gels immediately after the soluble precursors were mixed for up to 2 h. Twenty-minutes post mixing, G’ values increased from <5 Pa to approximately 150, 872, 12 and 89 Pa for DRC2, 4, 18 and 36, respectively. The value continued to rise gradually over time until the experiment was terminated at 2 h. All DRC gels are elastic, with the G” less than 5 Pa. When G’ is greater than 10×G”, a self-supporting viscoelastic solid is obtained.[17] The measured t_{10} value (Table 1) varies from 5.6 min for DRC4 to 18.3 min for DRC16. Such gelation kinetics provided a workable time window that ensures homogeneous distribution of hS/PCs in the crosslinked networks. At 2 h post mixing, an average G’ value of 808 ± 159, 1897 ± 81, 35 ± 2 and 216 ± 59 Pa was measured for DRC2, DRC4, DRC18 and DRC36 gels, respectively (Figure 2A). When the time sweep experiment was carried out on DRC18 beyond 2 h (Figure S2A), we observed a steady increase of G’ over time, reaching 76 ± 10 Pa by 6 h, suggesting that additional disulfide crosslinking is occuring. The corresponding tan(δ) (G”/G’) values were found to range from 0.02 to 0.002, indicating the elastic nature of the HA hydrogels. The storage moduli (Figure 2B) for DRC2, DRC4, and DRC36 were insensitive to frequency from 0.1 to 10 Hz, whereas DRC18 shows a marginal increase in modulus above 1 Hz possibly due to its relatively lower crosslinking density, and thereby longer relaxation time, as compared to other gel formulations.[18]

Hydrogel swelling (Figure 3A) was strongly dependent on the gel formulation, thiol/acrylate stoichiometry and incubation time. At 24 h, a swelling ratio of 29.2 ± 2.1, 27.0 ± 3.5, 82.4 ± 7.3, 108.6 ± 3.9 were measured for DRC2, DRC4, DRC18 and DRC36, respectively. The initial swelling was determined by the thiol/acrylate ratio, although the formation of disulfide bonds also contributes to the initial gelation (see below). Subsequent changes in gel swelling over the course of 28 days reflect the changes in network connectivity due to disulfide bond formation. The measured swelling ratio for all hydrogel formulations decreased from day 1 to day 4, with the values for DRC18 and DRC36 gels decreased dramatically by 53% and 64%, respectively, whereas DRC2 and DRC4 only experienced a moderate decrease (12% and 20%). Prolonged incubation beyond day 4 did not result in a significant change in swelling ratio. It should be noted that, compared to DRC4, DRC36 is more likely to form S-S crosslinks, its swelling ratio at day 28 (39.6 ± 1.3) is still

significantly ($p<0.05$) higher than that for DRC4 (21.8 ± 2.7). This can be attributed to the presence of simultaneous thiol/disulfide exchange reaction and the lower HA content in DRC36.

Analysis of the relative thiol content in each gel using DTNB (Figure 3B) revealed that, 2 h post mixing, approximately 40% and 60% of thiols were consumed for DRC18/DRC36 and DRC2/DRC4 gels, respectively. Our assay reveals that the disappearance of free thiols does not necessarily mean that they all become S-S, and under the experimental conditions, the conversion of thiols to sulfonates or sulfides is unlikely. Assuming all acrylate groups were consumed via Michael addition within 2 h of crosslinking, the percentage of thiols that form thioether bonds at 2 h would be 54.8%, 27.4%, 5.5% and 2.7% for DRC2, DRC4, DRC18 and DRC36, respectively. Based on these numbers, for DRC4, DRC18, and DRC36, it is evident that disulfide bonds are playing a large role in the network formation in the early stages of gelation. Although Michael addition is significantly faster than sulfhydryl oxidation,[15] both reactions contribute to the initial gelation, especially for DRC18 and DRC36 gels that exhibit a significant stoichiometric imbalance. Michael addition reaction brings free thiols into close proximity, thereby accelerating the S-S bond formation.[18] Thereafter, a continuous consumption of thiols was observed for DRC18 and DRC36 gels over the course of 7 days, reaching a 94 and 83% conversion respectively. Contrarily, >90% of the free thiols were rapidly consumed within 24 h for DRC2 and DRC4.

Finally, hydrogel degradation was analyzed indirectly by monitoring the amount of HA released in the supernatant from the hydrogel matrices (Figure 3C). At 24 h, ~0.5% and 5% HA was released from DRC2/DRC4 and DRC18/DRC36 gels, respectively, indicating a higher sol fraction for gels with a larger SH/AC mismatch. Prolonged incubation of DRC18 and DRC36 gels over the course of 28 days did not significantly increase HA release beyond that detected on day 1, indicating minimal gel degradation by ester hydrolysis as S-S bonds are the predominant crosslinking points in these gels. On the other hand, the DRC2 and DRC4 gels gradually released HA in a linear fashion, with an estimated 0.39 and 0.33% HA release per day respectively and reaching a cumulative HA release of 10.54 ± 0.54%, 9.60 ± 0.60%, respectively. These results are not surprising considering the fact that the Michael adduct, connected to the HA chains through 3 ester linkages, is the dominating crosslinking moieties in DRC2 and DRC4 gels. Overall, gels with a higher percentage of thiol/acrylate crosslinks degrade more readily because of their relative high content of ester linkages (Scheme 1).

3.2. 3D culture of MDCK cells in HA hydrogels

MDCK cells were employed as a robust ductal cell line to evaluate the suitability of the designed HA hydrogels for epithelial tissue morphogenesis. MDCK cells cultured in DRC gels form multicellular spheroids by day 7 in all four formulations (Figure 4), with spheroid size ranging from 30 to 175 μm. We further inspected MDCK cultures with the lowest thiol/acrylate ratio (DRC2) for cell viability, aggregation, morphology and polarization. As shown in Figure 5, MDCK cells, initially dispersed as single cells in the HA matrix, formed multicellular spherical aggregates on Day 3. The size of the spheroids increased over time, reaching an average diameter of 48 ± 14 μm by day 7 when the experiments were

terminated. By day 7, some spheroids contained PI-positive dead cells (red, Figure 5D) in the center of the structures, indicating the initiation of lumen formation via apoptosis.[19] Immunofluorescence results showed expression of β-catenin along the lateral membranes (Figure 5E), collagen IV localization on the basolateral membranes (Figure 5F) and apical localization of cortical F-actin (Figure 5G). Next, we analyzed a nuclear protein Ki67 that is present at all stages of cell division (G1, S, G2 and mitosis) except the resting stage (G0).[20] Highly abundant nuclear Ki67 among peripheral cells in the MDCK spheroids indicates active proliferation of cells within the spheroids (Figure 5G). Immunostaining also confirmed the presence of spheroids with a hollow lumen (white arrow, Figure 5E). Overall, MDCK cells readily assembled into organized 3D structures in DRC gels without added bioactive ECM-derived sequences or matrix metalloproteinase (MMP)-degradable sequence.

3.3. Formation of hS/PC spheroids in HA hydrogels

Next, we evaluated the effects of hydrogel compositions on the assembly of hS/PCs in 3D for up to 28 days. All four types of gel constructs remained as intact viscoelastic solids at the end of the culture (Figure S2B). Live/dead staining (Figure 6) revealed some compromised cell viability (stained red by PI) on day one, especially in DRC2 gels, possibly due to cell stress introduced during the encapsulation process and/or the high stiffness of DRC2. A comparable proportion of live cells (stained green by SYTO13) at day one were round and homogeneously distributed throughout the matrix. As time progressed, individual cells within the view field diminished and multicellular spheroid structures were formed. Viable multicellular structures were detected on day 14 in all four gel formulations, although spheroids in DRC2 gels were of low abundance and were smaller in size than those in other hydrogels. The size and the number of spheroids increased over time, and by day 28, the majority of cells residing in spheroids were alive, and dead cells were only found in individually dispersed single cell populations and those residing in the core of individual spheroids (see below). In general, spheroids in DRC18 and DRC36 were larger than those in DRC2 and DRC4 gels (Figure 6).

Spheroid size and morphology were assessed by confocal imaging after fluorescent staining for actin that clearly defined the bondaries of individual structures (Figure 7A). After 28 days of culture, hS/PC spheroids reached a median size of 32.9 ± 6.6, 29.7 ± 4.5, 50. 8 ± 9.3 and 57.1 ± 12.3 μm in DRC2, DRC4, DRC18 and DRC36 gels, respectively (Figure 7B). Although spheroids grown in DRC 2 and DRC 4 gels have a narrower size distribution (Figure 7B), these structures are small, mainly composed of less than ten cells per spheroid. On the other hand, DRC18 and 36 contain multicellular spheroids with dimensions exceeding 50 μm. Spheroid density was higher and the size distribution was narrower in DRC18 than in DRC36. These spheroids are not loose aggregates of multiple cells; they are organized entities with a compact spherical structure that are reminiscent of the basic acini units in the salivary gland.[21] Well organized spherical structures with cortical F-actin were detected in DRC18/DRC36 gels and individual spheroids contained multiple, closely packed cells with distinct nuclei and diminished cytoskeletal actin filaments. In sharp contrast, hS/PCs, when encapsulated in a similarly crosslinked HA hydrogel known to support spheroid formation for cancer cells,[9–10] remained as single cells throughout the culture for up to 28 days (Figure S3A) and eventually died, despite the gel's relatively low stiffness.

3.4. Characterization of hS/PC spheroids in HA hydrogels

hS/PCs grown in DRC18 gels were subjected to additional immunohistochemical analyses to evaluate cellular production of basement membrane components, cell-cell junction proteins, and stem/progenitor markers after 28 days of 3D culture. Characteristic and bright staining at the periphery of the organized spheroid structures was observed for collagen IV and laminin (Figure 8A, B), two of the most important structural proteins found in the basement membrane. Positive punctuated staining for occludin (Figure 8C) confirmed the presence of cell-cell and tight junctions in hS/PC spheroids. In addition, hS/PCs cultured in DRC18 gels expressed CD44, as evidenced from the confocal image (Figure 8D) and the flow cytometry results. Analysis of the relative mean geometric intensity showed that hS/PCs cultured in HA gels expressed 50% higher levels of CD44 compared to hS/PCs cultured on a 2D tissue culture dish (Table S2). Finally, intermediate filament proteins that are tightly associated with epithelial progenitor phenotype, K5 and K14, were both robustly expressed on the outer surface of hS/PC spheroids (Figure 8E, F). Smaller structures grown in DRC2 and DRC4 were also stained positive for K5 and K14 (Figure S3C). Our previous work[13] show that these markers are persistently expressed and maintained from the expanded cell population throughout the 3D culture. Collectively, these results show that hS/PCs cultured in the hydrogel are metabolically active, phenotypically stable and morphologically similar to the lobular structures found in the native tissue.

Quantification by PicoGreen dsDNA assay (Figure 9A) shows that hS/PCs proliferated by 2.4 ± 0.1, 1.5 ± 0.7, 3.8 ± 0.3 and 2.7 ± 0.3 folds from day 0 to day 28 in DRC2, DRC4, DRC18 and DRC36 gels, respectively. Overall, cells are signficantly ($p<0.05$) more proliferative in DRC18 gels than in other gel formulations. Cells grown in DRC18 gels stained positive for Ki67 (Figure 9B) and Ki67+ cells were located closer to the outer surface of the structures. In additon, positive cleaved caspase 3 staining, an indicator of cell apoptosis, was detected at the center of the spheroids (Figure 9C). Live/dead staining also revealed the presence of centrally located dead cells surrounded by live cells that form tight contacts with each other (Figure S3D). Collectively, these results indicate that DRC18 gels not only facilitate hS/PC proliferation but also guide cell proliferation and selective apoptosis, depending on the cellular localization within the organized 3D structures.

4. Discussion

Reconstitution of functional salivary gland units in a biocompatible hydrogel matrix with long-term *in vivo* stability is a key step toward creation of an implantable functional salivary gland. Acini-like lobules with intimate cell-cell contacts seen in the native tissue must be recapitulated in the engineered, multicellular units to enable fluid secretion upon neurotransmitter stimulation. Although multicellular spheroids can be produced through scaffold-free 3D culture methods, e.g. low attachment culture, spinning flask and hanging drop, spheroids assembled from singly dispersed cells in the presence of a synthetic matrix are more physiologically relevant owing to the intimate contact of cells with the matrix components. It is well accepted that cell-ECM interactions critically mediate cell growth, survival, differentiation and morphogenesis. The biochemical factors sequestered in the ECM and the mechanical forces generated through the ECM regulate cell behaviors, which

in turn, sculpt and stabilize the epithelial tissue structure. The presence of synthetic ECM also helps retain and sequester cell-secreted proteins, further reinforcing the cell-matrix interactions.[22–25] 3D culture of human or mouse salivary gland stem/progenitor cells has been attempted using animal-derived matrices, such as Matrigel,[26] fibrin hydrogel,[27] collagen I,[28] and decellularized scaffolds.[29] These scaffolds are non-human compatible and their mechanical and chemical properties cannot be easily adjusted.

We are the first to successfully isolate, expand and culture hS/PCs in covalently crosslinked hydrogel gels. Using HA of high (500 kDa) and low (5 kDa) molecular weight, hydrogels with varying thiol/acrylate ratio (2/1 to 36/1), network connectivity and stiffness (G' of 35 to 1897 Pa, 2 h post mixing) were established rapidly upon mixing of concentrated stock solutions at a constant volumetric ratio. The stiffness of the DRC gels is dependent on the network connectivity and HA content. Compared to DRC2 and DRC4, DRC18 has a lower acrylate concentration and HA content, therefore a lower modulus. Compared to DRC36, DRC18 contains the same amount of acrylate groups, but a lower thiol concentration and HA content. With the same acrylate concentration, a higher thiol content leads to a more rapid consumption of the acrylate groups and more abundant S-S bridges to connect more HA chains in DRC36. Consequently, DRC18 is softer than DRC36 2 h post mixing. Despite its higher modulus, DRC36 initially swells to a lesser degree than DRC18, owing to the larger percentage of dangling HA chains in DRC36. Because S-S bond forms readily in both DRC18 and DRC36, the swelling ratio for both gels merged to approximately 40 by day 28.

For 3D culture of normal epithelial cells, it is desirable that the synthetic matrix exhibit time-dependent dynamic features to promote the cell growth and to accommodate spheroid expansion. Work from other groups has led to the development of synthetic hydrogels that became stiffen over time, either spontaneously or via an external trigger. These materials are designed to mimic the stiffening of matrix during development, wound healing and disease.[30–32] In our design, simultaneous formation of the disulfide crosslinks complements the thioether linkages in the HA network to ensure rapid gelation, although the initial gel stiffness is predominantly determined by the thioether network. The Michael reaction continued well beyond the gelation point for up to 90 min, during which period, the elastic modulus increased moderately. The residual free thiols in DRC2 and DRC4 gels were converted to S-S rapidly within 24 h, whereas those in DRC18 and DRC36 gels became oxidized slowly over the course of 7 days. Using a significantly large excess of thiol relative to acrylate, our goal is to rapidly establish a primary thioether-based network that can be gradually remodeled by the disulfide crosslinks to accommodate the growth of hS/PCs and expansion of the spheroids. In addition, the thiol/acrylate crosslinks are hydrolytically degradable,[33] and networks containing a higher percentage of ester linkages (DRC2/DRC4) are more susceptible to hydrolysis. Such a dynamically evolving network provides a mechanically and biologically relevant microenvironment that is favorable for the organized growth of lobular structures.

The morphogenesis of MDCK cells has been extensively studied and many findings reported using this cell line has been validated both *in vitro* and *in vivo*.[34–37] Our initial experiments show that MDCK cells formed multicellular spherical aggregates rapidly in all four types of DRC gels. Further morphological analysis of MDCK spheroids in DRC2, one of the

disulfide-lean gel formulations with a 2-h G' value of approximately 800 Pa, confirmed the ability of individually dispersed single cells to form these organized structures with central lumen. Thus, DRC gels provide a biologically relevant microenvironment that initiates the desired morphogenesis for MDCK cells.[38] Of note, the DRC gels are purely HA-based and devoid of any MMP-degradable linkers or integrin binding peptide (IBP) ligands. Other researchers have found that MDCK cells, encapsulated within PEG-based hydrogels required both MMP and IBP signals to elicit the formation of properly polarized cysts.[39] These results imply that MDCK cells may interact with the HA network (via the cell surface HA binding proteins or HAase) to activate signaling pathways that promote the cellular secretion of basement membrane proteins, leading to the establishment of organized multicellular structures.

The positive MDCK results motivated us to explore the 3D culture of hS/PCs in the new HA hydrogels. Immediately after cell encapsulation, moderate cell death was observed in DRC2 gels, the most non-permissive formulations for hS/PCs. The absence of cell-cell contacts in these singly dispersed primary epithelial progenitor cells renders them susceptible to physical trauma. In the most conducive gels (DRC18), however, individual cells making up an organized spheroids are highly viable, except those residing in the core of the spheroids, potentially initiating the formation of a hollow lumen. Because the establishment of organized spherical assemblies from dispersed hS/PCs is the first step towards the generation of functional glandular units, our primary goal is to understand how experimental parameters and matrix properties affect the growth and organization of hS/PC spheroids. In our study, hS/PC cultures were terminated once organized spheroids reached a phsyiologically relevant dimensions of 50 μm, a pre-requisite for the proper function of salivary gland epithelial cells[12, 21] Prolonged incubation of spheroid-laden hydrogel will likely lead to merging of neighboring structures without structural reorganization.[13] The utility of the DRC gels is gauged by the ability of the resident hS/PCs to reach this critical dimension within the time frame of the experiments.

Among four hydrogel formulations investigated, the stiffer and disulfide-lean hydrogels, DRC2/DRC4 gels, although more susceptible to hydrolytic degradation, do not promote the formation of large organized spheroids from dispersed hS/PCs. The softer and disulfide-rich hydrogels, DRC18/DRC36, provide a more permissive environment for hS/PC assembly. The slow kinetics of disulfide bond formation and the high degree of gel swelling during the initial period of 3D culture allows encapsulated hS/PCs to expand within the matrix to form organized acini structures. It is notable that these reactions do not compromise the overall integrity of the DRC18 hydrogel matrix. Our comparative studies show that hS/PCs form a higher number of spheroids with uniform spheroid size distribution in gels that are softer and have a larger excess of thiols relative to acrylates. hS/PCs cultured in these gels formed well-defined spheroids with characteristic cell-cell contacts that are crucial for epithelial organization. Spheroids in DRC36 are less abundant and more broadly distributed than those found in DRC18 and cells in DRC36 do not proliferate as readily as those in DRC18. The spheroid size does not correlate positively with cell proliferation. Previous studies on breast epithelium showed that formation of epithelial spheroid structures in hydrogels is a combination of cell proliferation, rotation and migration.[40] The PicoGreen assay confirmed cell proliferation in our 3D matrices, and Ki67 immunostaining revealed cell cycle

progression for a significant proportion of aggregated cells. Intriguingly, by day 28, some spheroids were found to contain a PI and cleaved caspase 3-positive central core, indicating the initiation of lumen formation.[41] In adult salivary glands, the secretory acini located at the end bud has a spheroid structure with a central lumen that is polarized with an apical cell membrane and transmembrane pores, such as aquaporin 5 (AQP5) and Na^+/K^+ Pumps.[42–43] Thus, structures formed in DRC18 gels are morphologically analogous to the structural units found in the native tissues, but their apicobasal polarization is still to be determined.[13, 44]

The ability of HA-based hydrogels to maintain the stem cell phenotype and to support lineage specific differentiations when soluble factors are introduced have been documented.[45] Our recent investigations showed that primary human salivary gland cells isolated from freshly resected surgical tissues express stem/progenitor cell markers. The progenitor marker expression is maintained in 2D for over 15 passages and in 3D for over 118 days. Essentially all spheroids grown in the 3D HA-based hydrogels were stained positive for stem/progenitor markers.[13] Similarly, the stem/progenitor markers are maintained in all DRC cultures irrespective of the spheroid dimensions. The DRC18 gels not only supported robust and consistent spheroid formation from dispersed hS/PCs, but also contributed to the stable maintenance of a stem/progenitor cell phenotype. Cells in the 3D structures expressed epithelial progenitor markers, K5 and K14, and could be induced to differentiate toward an acinar phenotype when properly stimulated. The cell-surface localization of an additional stem cell marker, CD44, attests to the stem-like nature of cells in our culture, again in agreement with our previous observations.[44]

These observations imply that the multipotent hS/PCs structures developed in the DRC18 gels may be used to generate the entire gland given the appropriate signaling and stimulatory cues needed for differentiation and functionality. In future studies, we intend to induce branching morphogenesis from the organized spheroids and subsequently differentiate stem/progenitor cells residing in the branched structures into specialized salivary gland lineages with secretory and transport properties. The ultimate goal is to recreate salivary gland acini-like lobules attached to elongated ductal structures.

5. Conclusions

We have developed a novel adaptable hydrogel platform suitable for the 3D culture and assembly of primary human salivary stem/progenitor cells. The covalent network contains varying proportions of stable thioether bonds with neighboring ester groups and adaptable disulfide linkages. hS/PCs embedded in the matrices as single cells form organized structures resembling those found in the native glands. The proliferative capacity of hS/PCs, the frequency of spheroid formation and the size of the spheroids developed are strongly dependent on the gel formulations, with those containing the least amount of HA (1wt%) and an intermediate thiol/acrylate ratio of (18/1) being the most permissive and conducive. Cells in the assembled spheroids are viable, proliferative and phenotypically stable, exhibiting differential proliferation and apoptosis patterns. Altogether, these custom designed HA hydrogels exhibit unique network connectivity with a unique stress relaxation mechanism, thereby promoting cell migration and proliferation in the nanoporous

framework. Ongoing work is dedicated to the establishment of microenvironmental cues that support specific differentiation of all cell types needed to fully restore the salivary gland.

Supplementary Material

Refer to Web version on PubMed Central for supplementary material.

Acknowledgments

The authors wish to acknowledge Genzyme for generously providing HA. We thank Mr. Chen-Yuan Kao from the Papoutsakis Lab for his assistance with FACS experiments, Dr. Shi Bai for his advice on the HR-MAS ^{1}H NMR experiment and Dr. Jeff Caplan for his guidance on confocal imaging. We thank all of our laboratory members and collaborators for many helpful discussions. This work was supported in part by National Institutes of Health (NIDCR, R01 DE022969) (to DH, RLW, MCFC, SPB, XJ), Delaware Bioscience Center for Advanced Technology (to XJ) and DuPont (to XJ). We acknowledge the Delaware COBRE program (NIGMS: P30 GM110758) for instrumentation support.

References

1. Fajardo LF, Berthrong M. Radiation injury in surgical pathology. Part III. Salivary glands, pancreas and skin. Am J Surg Pathol. 1981; 5(3):279–296. [PubMed: 7235121]
2. Siegel RL, Miller KD, Jemal A. Cancer statistics, 2016. CA Cancer J Clin. 2016; 66(1):7–30. [PubMed: 26742998]
3. Nagler RM, Baum BJ. Prophylactic treatment reduces the severity of xerostomia following radiation therapy for oral cavity cancer. Arch Otolaryngol Head Neck Surg. 2003; 129:247–250. [PubMed: 12578459]
4. Witt, RL. Salivary gland diseases: surgical and medical management. New York: Thieme; 2005. p. xvp. 272
5. Chitturi RT, Veeravarmal V, Nirmal RM, Reddy BV. Myoepithelial Cells (MEC) of the Salivary Glands in Health and Tumours. J Clin Diagn Res. 2015; 9(3):ZE14–ZE18.
6. Ozdemir T, Fowler EW, Hao Y, Ravikrishnan A, Harrington DA, Witt RL, Farach-Carson MC, Pradhan-Bhatt S, Jia X. Biomaterials-based strategies for salivary gland tissue regeneration. Biomater Sci. 2016; 4(4):592–604. [PubMed: 26878077]
7. Shubin AD, Felong TJ, Graunke D, Ovitt CE, Benoit DS. Development of poly(ethylene glycol) hydrogels for salivary gland tissue engineering applications. Tissue Eng Part A. 2015; 21(11–12): 1733–1751. [PubMed: 25762214]
8. Xu X, Farach-Carson MC, Jia X. Three-dimensional in vitro tumor models for cancer research and drug evaluation. Biotechnol Adv. 2014; 32(7):1256–1268. [PubMed: 25116894]
9. Xu X, Gurski LA, Zhang C, Harrington DA, Farach-Carson MC, Jia X. Recreating the tumor microenvironment in a bilayer, hyaluronic acid hydrogel construct for the growth of prostate cancer spheroids. Biomaterials. 2012; 33(35):9049–9060. [PubMed: 22999468]
10. Xu X, Sabanayagam CR, Harrington DA, Farach-Carson MC, Jia X. A hydrogel-based tumor model for the evaluation of nanoparticle-based cancer therapeutics. Biomaterials. 2014; 35(10): 3319–3330. [PubMed: 24447463]
11. Zhang H, Dicker KT, Xu X, Jia X, Fox JM. Interfacial Bioorthogonal Cross-Linking. ACS Macro Lett. 2014; 3(8):727–731. [PubMed: 25177528]
12. Pradhan-Bhatt S, Harrington DA, Duncan RL, Jia X, Witt RL, Farach-Carson MC. Implantable three-dimensional salivary spheroid assemblies demonstrate fluid and protein secretory responses to neurotransmitters. Tissue Eng Part A. 2013; 19(13–14):1610–1620. [PubMed: 23442148]
13. Srinivasan PP, Patel VN, Liu S, Harrington DA, Hoffman MP, Jia X, Witt RL, Farach-Carson MC, Pradhan-Bhatt S. Primary Salivary Human Stem/Progenitor Cells Undergo Microenvironment-Driven Acinar-Like Differentiation in Hyaluronate Hydrogel Culture. Stem Cells Transl Med. 2016

14. Dicker KT, Gurski LA, Pradhan-Bhatt S, Witt RL, Farach-Carson MC, Jia X. Hyaluronan: a simple polysaccharide with diverse biological functions. Acta Biomater. 2014; 10(4):1558–1570. [PubMed: 24361428]
15. Shu XZ, Liu YC, Luo Y, Roberts MC, Prestwich GD. Disulfide cross-linked hyaluronan hydrogels. Biomacromolecules. 2002; 3(6):1304–1311. [PubMed: 12425669]
16. Bitter T, Muir HM. A modified uronic acid carbazole reaction. Analytical Biochemistry. 1962; 4(4):330–334. [PubMed: 13971270]
17. Sperling, LH. Introduction to Physical Polymer Science. 4th. Hoboken, NJ: Wiley-Interscience; 2006.
18. Ghosh K, Shu XZ, Mou R, Lombardi J, Prestwich GD, Rafailovich MH, Clark RA. Rheological characterization of in situ cross-linkable hyaluronan hydrogels. Biomacromolecules. 2005; 6(5): 2857–2865. [PubMed: 16153128]
19. Sigurbjornsdottir S, Mathew R, Leptin M. Molecular mechanisms of de novo lumen formation. Nature Reviews Molecular Cell Biology. 2014; 15(10):665–676. [PubMed: 25186133]
20. Urruticoechea A, Smith IE, Dowsett M. Proliferation marker Ki-67 in early breast cancer. J Clin Oncol. 2005; 23(28):7212–7220.
21. Pradhan-Bhatt, S.; Cannon, K.; Zakheim, D.; Harrington, DA.; Duncan, RL.; Jia, X.; Farach-Carson, MC.; Witt, RL. Salivary Gland Tissue Engineering and Repair. In: Vishwakarma, APS.; Sharpe, S.; Ramalingham, M., editors. Stem Cell Biology and Tissue Engineering in Dental Sciences. Elsevier; 2015. p. 613-623.
22. Harunaga J, Hsu JC, Yamada KM. Dynamics of salivary gland morphogenesis. J Dent Res. 2011; 90(9):1070–1077. [PubMed: 21487116]
23. Heisenberg CP, Bellaiche Y. Forces in tissue morphogenesis and patterning. Cell. 2013; 153(5): 948–962. [PubMed: 23706734]
24. Daley WP, Yamada KM. ECM-modulated cellular dynamics as a driving force for tissue morphogenesis. Curr Opin Genet Dev. 2013; 23(4):408–414. [PubMed: 23849799]
25. Rozario T, DeSimone DW. The extracellular matrix in development and morphogenesis: a dynamic view. Dev Biol. 2010; 341(1):126–140. [PubMed: 19854168]
26. Leigh NJ, Nelson JW, Mellas RE, McCall AD, Baker OJ. Three-dimensional cultures of mouse submandibular and parotid glands: a comparative study. J Tissue Eng Regen Med. 2014
27. McCall AD, Nelson JW, Leigh NJ, Duffey ME, Lei P, Andreadis ST, Baker OJ. Growth factors polymerized within fibrin hydrogel promote amylase production in parotid cells. Tissue Eng Part A. 2013; 19(19–20):2215–2225. [PubMed: 23594102]
28. Joraku A, Sullivan CA, Yoo J, Atala A. In-vitro reconstitution of three-dimensional human salivary gland tissue structures. Differentiation. 2007; 75(4):318–324. [PubMed: 17376117]
29. Gao Z, Wu T, Xu J, Liu G, Xie Y, Zhang C, Wang J, Wang S. Generation of Bioartificial Salivary Gland Using Whole-Organ Decellularized Bioscaffold. Cells Tissues Organs. 2014; 200(3–4):171–180. [PubMed: 25824480]
30. Young JL, Engler AJ. Hydrogels with time-dependent material properties enhance cardiomyocyte differentiation in vitro. Biomaterials. 2011; 32(4):1002–1009. [PubMed: 21071078]
31. Guvendiren M, Burdick JA. Stiffening hydrogels to probe short- and long-term cellular responses to dynamic mechanics. Nat Commun. 2012; 3:792. [PubMed: 22531177]
32. Mabry KM, Lawrence RL, Anseth KS. Dynamic stiffening of poly(ethylene glycol)-based hydrogels to direct valvular interstitial cell phenotype in a three-dimensional environment. Biomaterials. 2015; 49:47–56. [PubMed: 25725554]
33. Rydholm AE, Anseth KS, Bowman CN. Effects of neighboring sulfides and pH on ester hydrolysis in thiol-acrylate photopolymers. Acta Biomater. 2007; 3(4):449–455. [PubMed: 17276150]
34. Fan C, Miao Y, Zhang X, Liu D, Jiang G, Lin X, Han Q, Luan L, Xu Z, Wang E. Btbd7 contributes to reduced E-cadherin expression and predicts poor prognosis in non-small cell lung cancer. BMC Cancer. 2014; 14:704. [PubMed: 25253020]
35. Bandyopadhyay BC, Swaim WD, Liu X, Redman RS, Patterson RL, Ambudkar IS. Apical localization of a functional TRPC3/TRPC6-Ca2+-signaling complex in polarized epithelial cells. Role in apical Ca2+ influx. J Biol Chem. 2005; 280(13):12908–12916. [PubMed: 15623527]

36. Wells EK, Yarborough O 3rd, Lifton RP, Cantley LG, Caplan MJ. Epithelial morphogenesis of MDCK cells in three-dimensional collagen culture is modulated by interleukin-8. Am J Physiol Cell Physiol. 2013; 304(10):C966–C975. [PubMed: 23485708]
37. Delporte C, O'Connell BC, He X, Lancaster HE, O'Connell AC, Agre P, Baum BJ. Increased fluid secretion after adenoviral-mediated transfer of the aquaporin-1 cDNA to irradiated rat salivary glands. Proc Natl Acad Sci U S A. 1997; 94(7):3268–3273. [PubMed: 9096382]
38. Schluter MA, Margolis B. Apical lumen formation in renal epithelia. J Am Soc Nephrol. 2009; 20(7):1444–1452. [PubMed: 19497970]
39. Chung IM, Enemchukwu NO, Khaja SD, Murthy N, Mantalaris A, Garcia AJ. Bioadhesive hydrogel microenvironments to modulate epithelial morphogenesis. Biomaterials. 2008; 29(17): 2637–2645. [PubMed: 18377982]
40. Tanner K, Mori H, Mroue R, Bruni-Cardoso A, Bissell MJ. Coherent angular motion in the establishment of multicellular architecture of glandular tissues. Proc Natl Acad Sci U S A. 2012; 109(6):1973–1978. [PubMed: 22308439]
41. Boatright KM, Salvesen GS. Mechanisms of caspase activation. Curr Opin Cell Biol. 2003; 15(6): 725–731. [PubMed: 14644197]
42. Wells KL, Patel N. Lumen formation in salivary gland development. Front Oral Biol. 2010; 14:78–89. [PubMed: 20428012]
43. Pradhan S, Liu C, Zhang C, Jia X, Farach-Carson MC, Witt RL. Lumen formation in three-dimensional cultures of salivary acinar cells. Otolaryngol Head Neck Surg. 2010; 142(2):191–195. [PubMed: 20115973]
44. Pradhan-Bhatt S, Harrington DA, Duncan RL, Farach-Carson MC, Jia X, Witt RL. A novel in vivo model for evaluating functional restoration of a tissue-engineered salivary gland. Laryngoscope. 2014; 124(2):456–461. [PubMed: 23832678]
45. Gerecht S, Burdick JA, Ferreira LS, Townsend SA, Langer R, Vunjak-Novakovic G. Hyaluronic acid hydrogel for controlled self-renewal and differentiation of human embryonic stem cells. Proc Natl Acad Sci U S A. 2007; 104(27):11298–11303. [PubMed: 17581871]

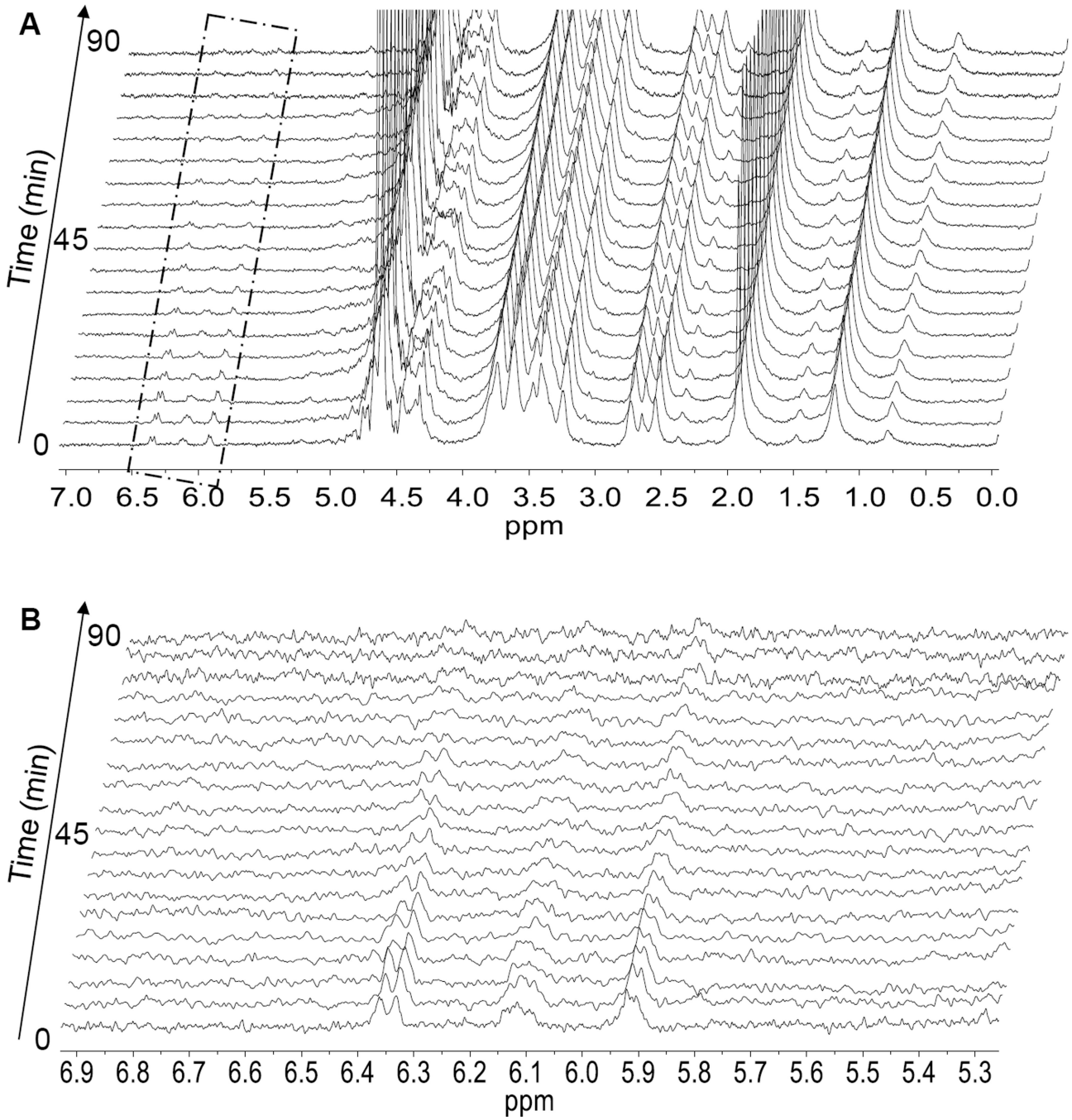

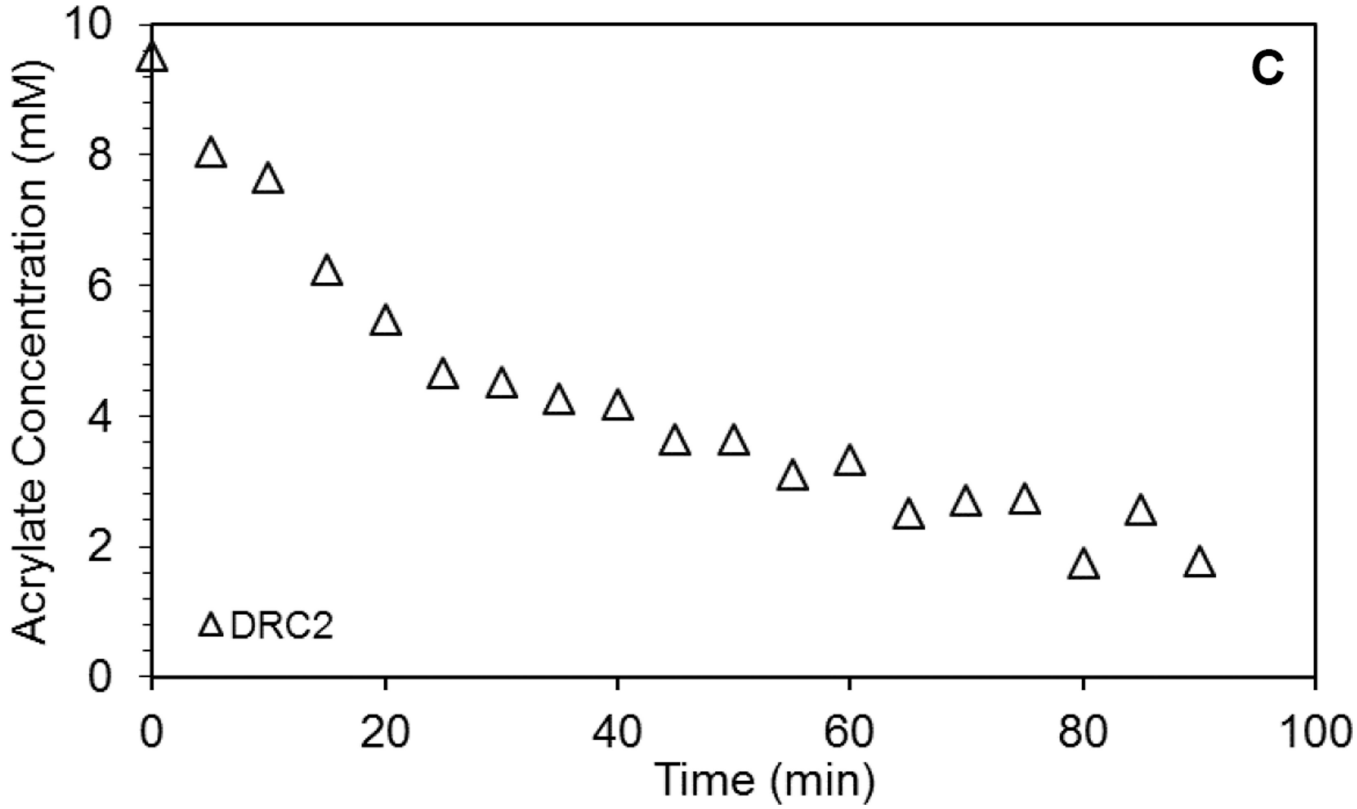

Figure 1.

Characterization of acrylate group consumption in DRC2 gels by high resolution magic angle spinning (HR-MAS) ^{1}H NMR. (A–B) ^{1}H NMR spectra resolved at five minute increments for 90 minutes. Regions of the vinyl protons (boxed area in A) are enlarged in B. (C) Reduction of acrylate concentration in the hydrogel as a function of time after the hydrogel precursors were mixed. Acrylate concentration determined from the integration of the vinyl protons at 6.33, 6.10, and 5.89 ppm.

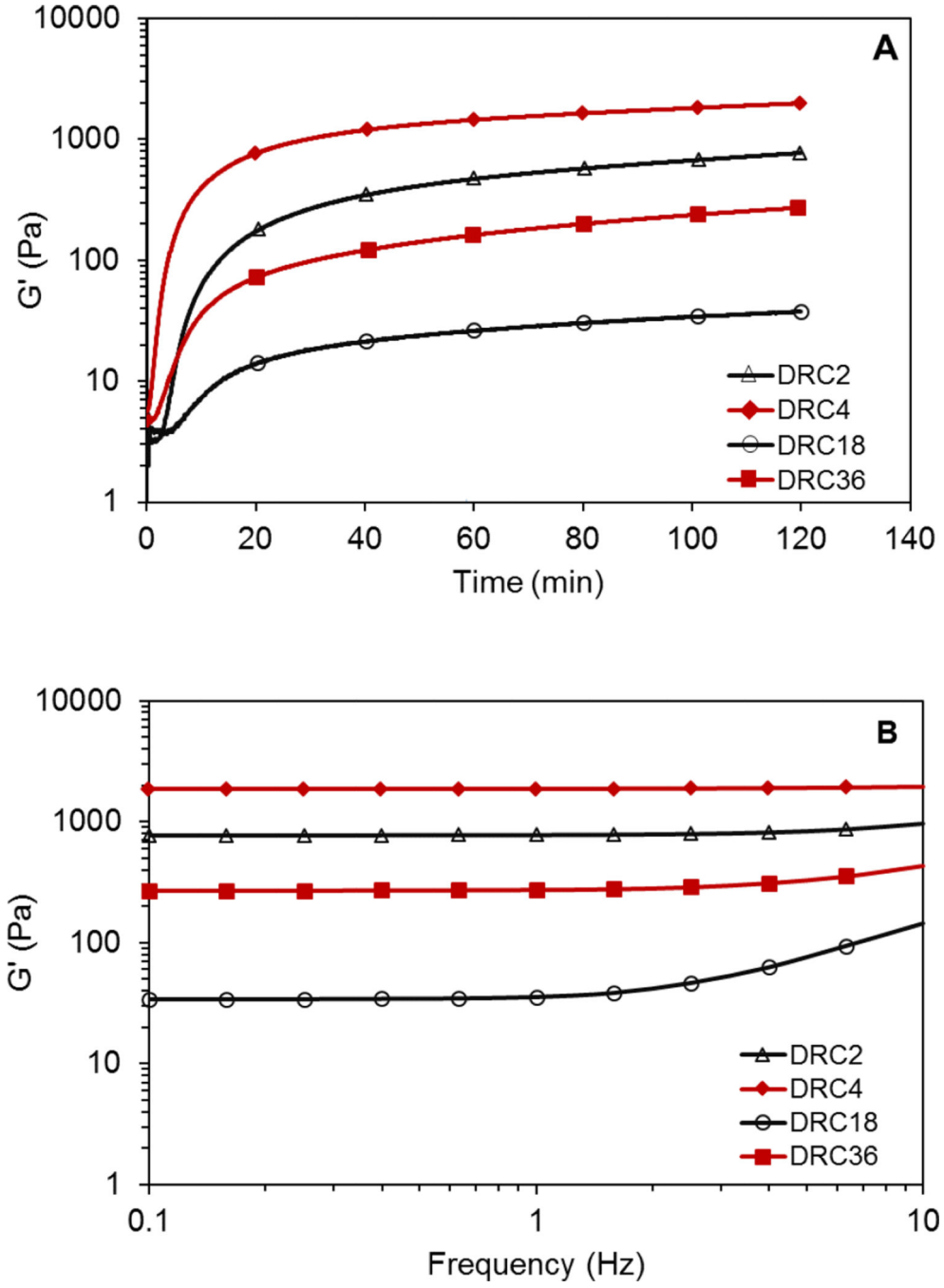

Figure 2.

Representative rheological measurements of HA hydrogels (DRC2: △; DRC4: ◆; DRC18: ○ and DRC36: ■). (A): Time sweep; (B): Frequency sweep. Samples were loaded on the geometry immediately after HA-SH and HA-AES were mixed. Frequency sweep was carried out immediately after the time sweep, i.e. 2 h post mixing.

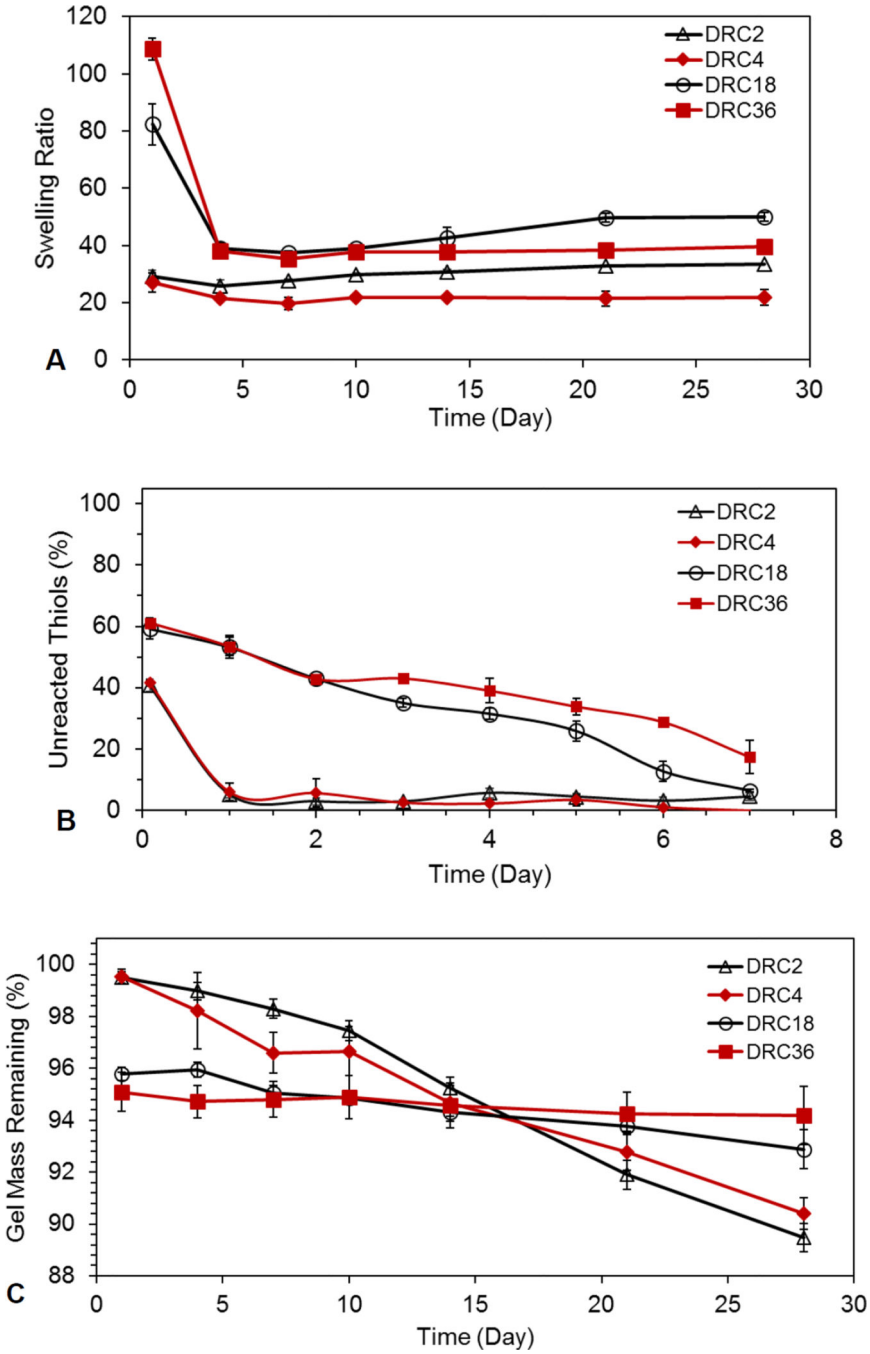

Figure 3.

Characterization of time-dependent hydrogel properties (DRC2: △; DRC4: ◆; DRC18: ○ and DRC36: ■). (A): Swelling ratio as a function of incubation time in PBS at 37 °C. The swelling ratio was determined gravimetrically. (B) Consumption of free thiols as a function of incubation time at 37 °C. Thiol concentration was analyzed via absorbance at 405 nm from the stoichiometric reaction of DTNB with thiols. (C) Gel mass as a function of time. Gel mass was calculated based on HA released into the supernatant using carbazole assay. The first data sets represent the values at 2 h post mixing.

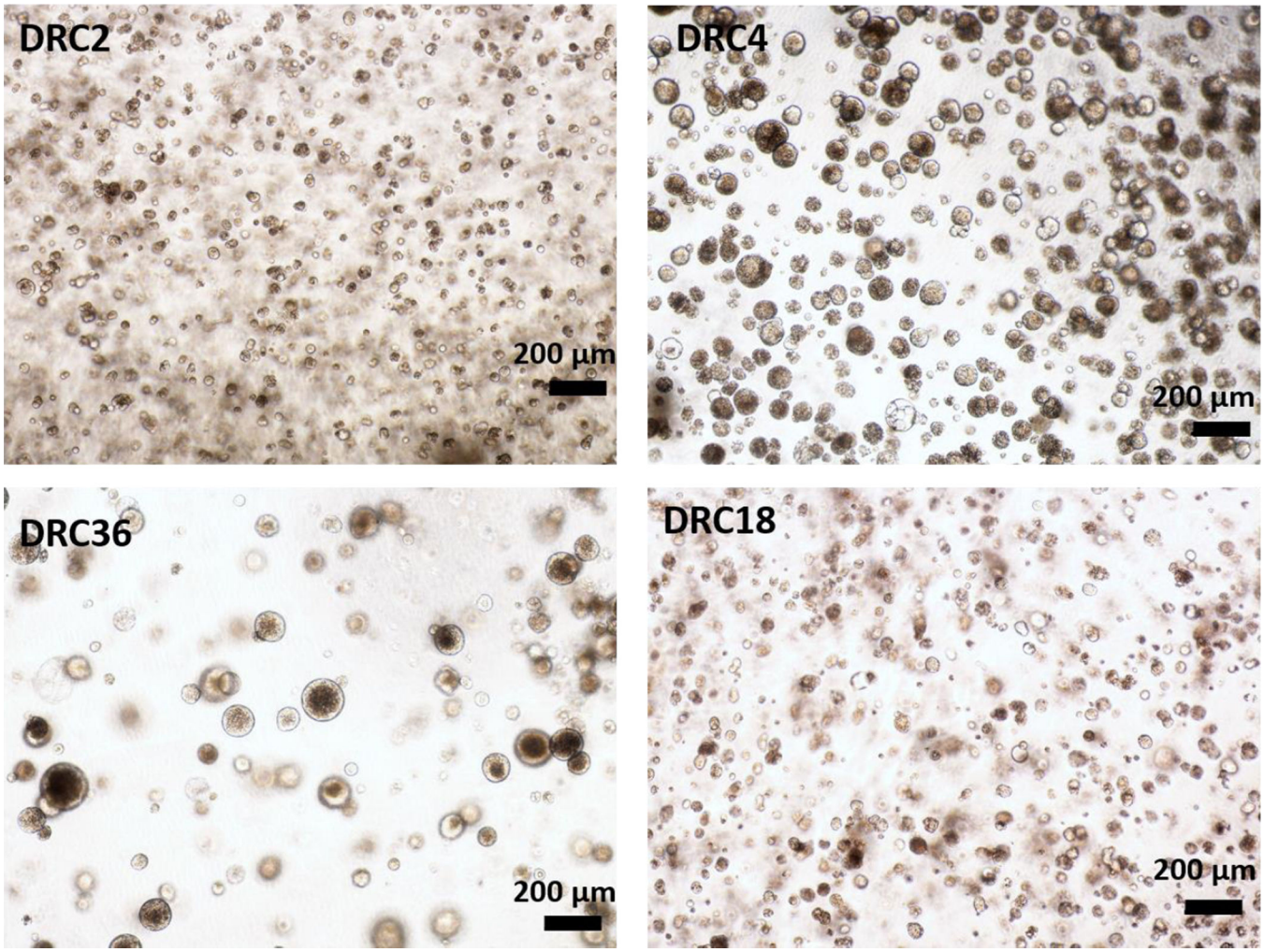

Figure 4.

Representative bright field images of MDCK cells encapsulated in DRC2, 4, 18 and 36 hydrogels. MDCK cells formed multicellular spheroids readily with varying sizes after 7 days of culture (Magnification: 5×).

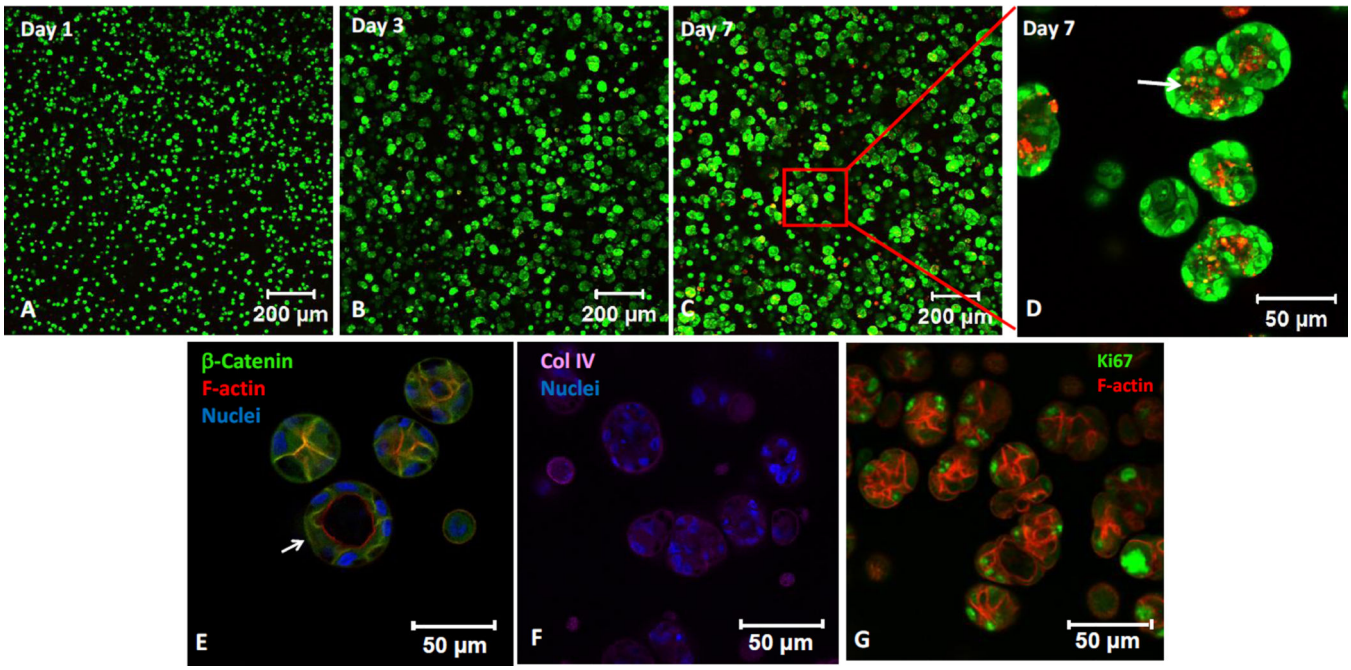

Figure 5.

Characterization of MDCK spheroids grown in DRC2 gels by immunofluorescence and confocal imaging. (A–D): Live (green) and dead (red) cells were stained with SYTO-13 and propidium iodide, respectively. Boxed region in C is shown at a higher magnification in D. White arrow in D indicates dead cells in the center of a spheroid. (E–H): Day 7 MDCK spheroids were immunostained for β-catenin (E, green), collagen IV (F, purple) and Ki67 (H, green). F-actin and nuclei were stained red and blue by phalloidin and DAPI, respectively. White arrow in E points to a spheroid with a hollow lumen.

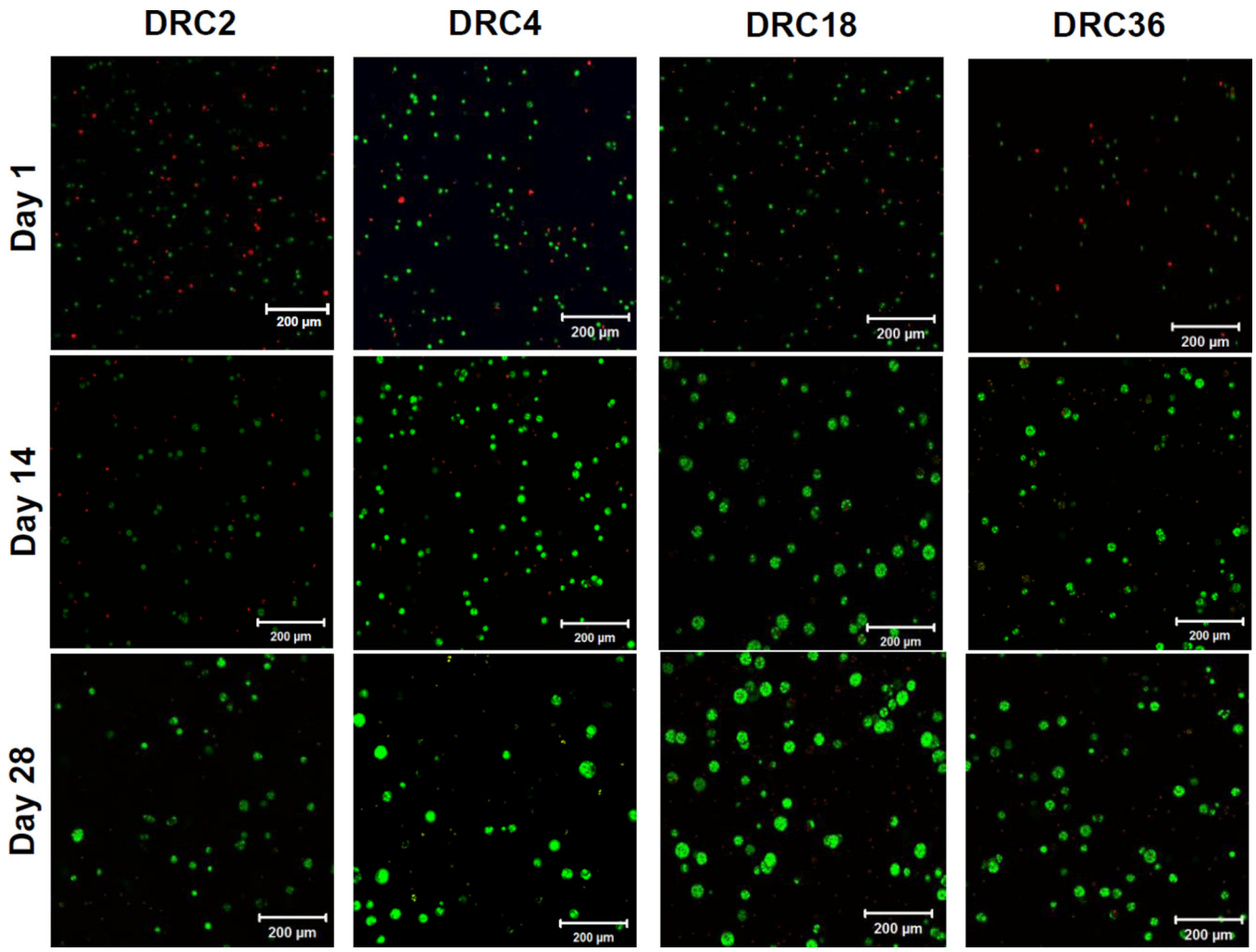

Figure 6.

Representative confocal images of live/dead stained hS/PCs cells cultured in the respective HA hydrogels on day 1, 14 and 28. Live (green) and dead (red) cells were stained with SYTO-13 and PI, respectively. The 200 μm thick sections with 1-μm increments were de-convoluted using maximum intensity projection.

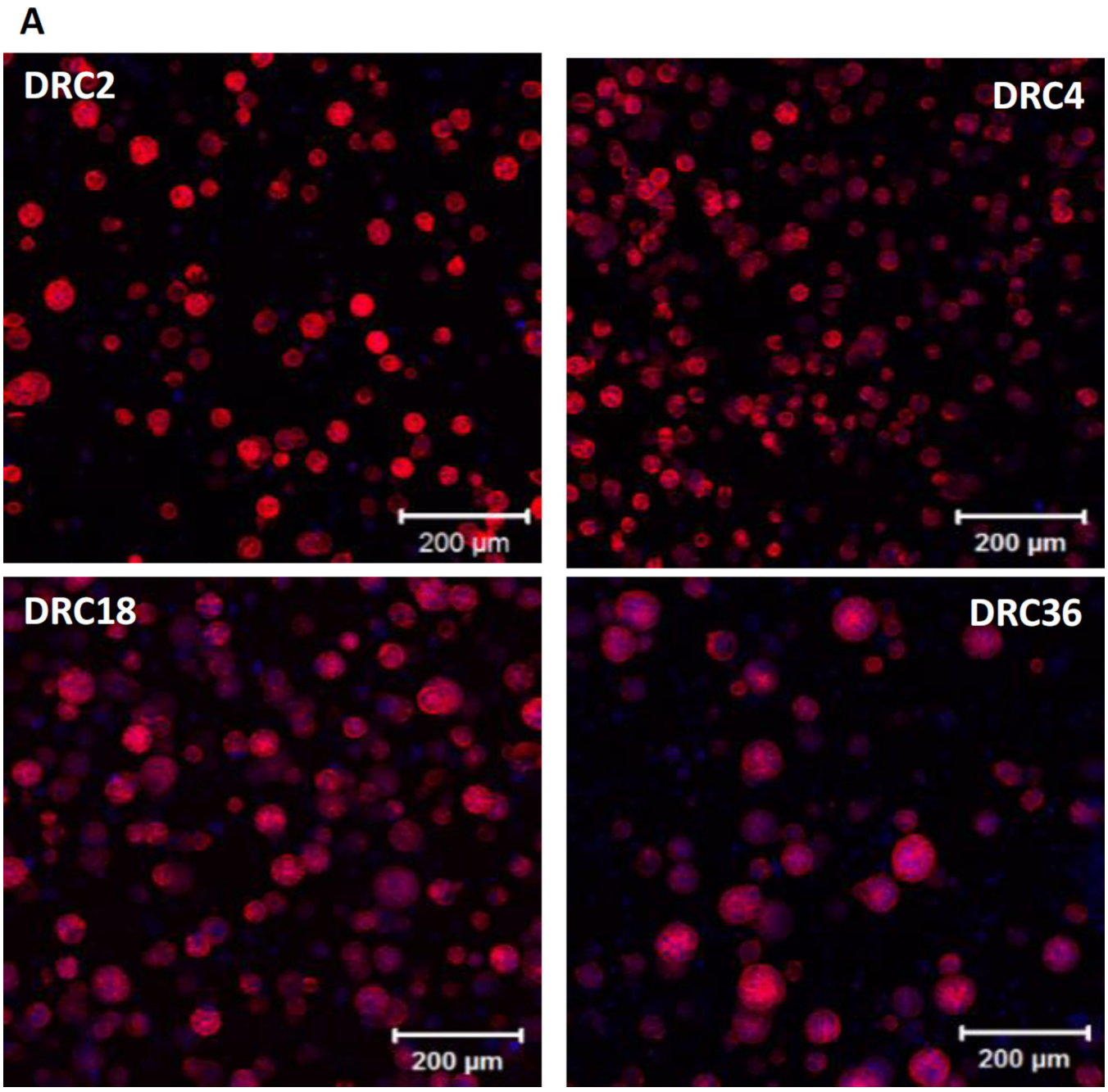

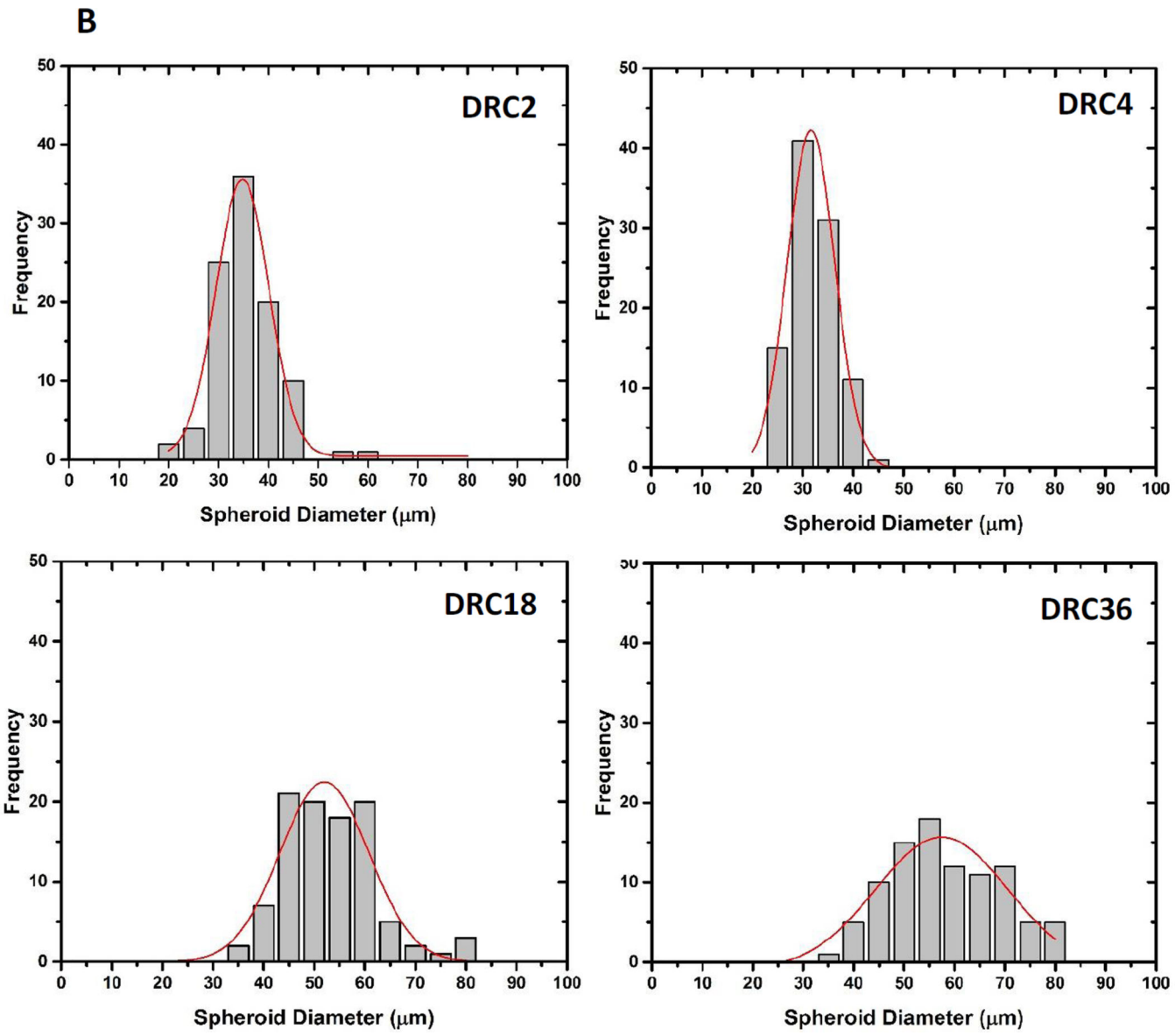

Figure 7.

Characterization of hS/PC spheroid size after 28 days of culture in the respective HA hydrogels. (A) Confocal images of fluorescently stained hS/PCs. Cell nuclei and F-actin were stained blue and red, respectively. (B) Gaussian fit of spheroid size distribution in each gels from the respective confocal images.

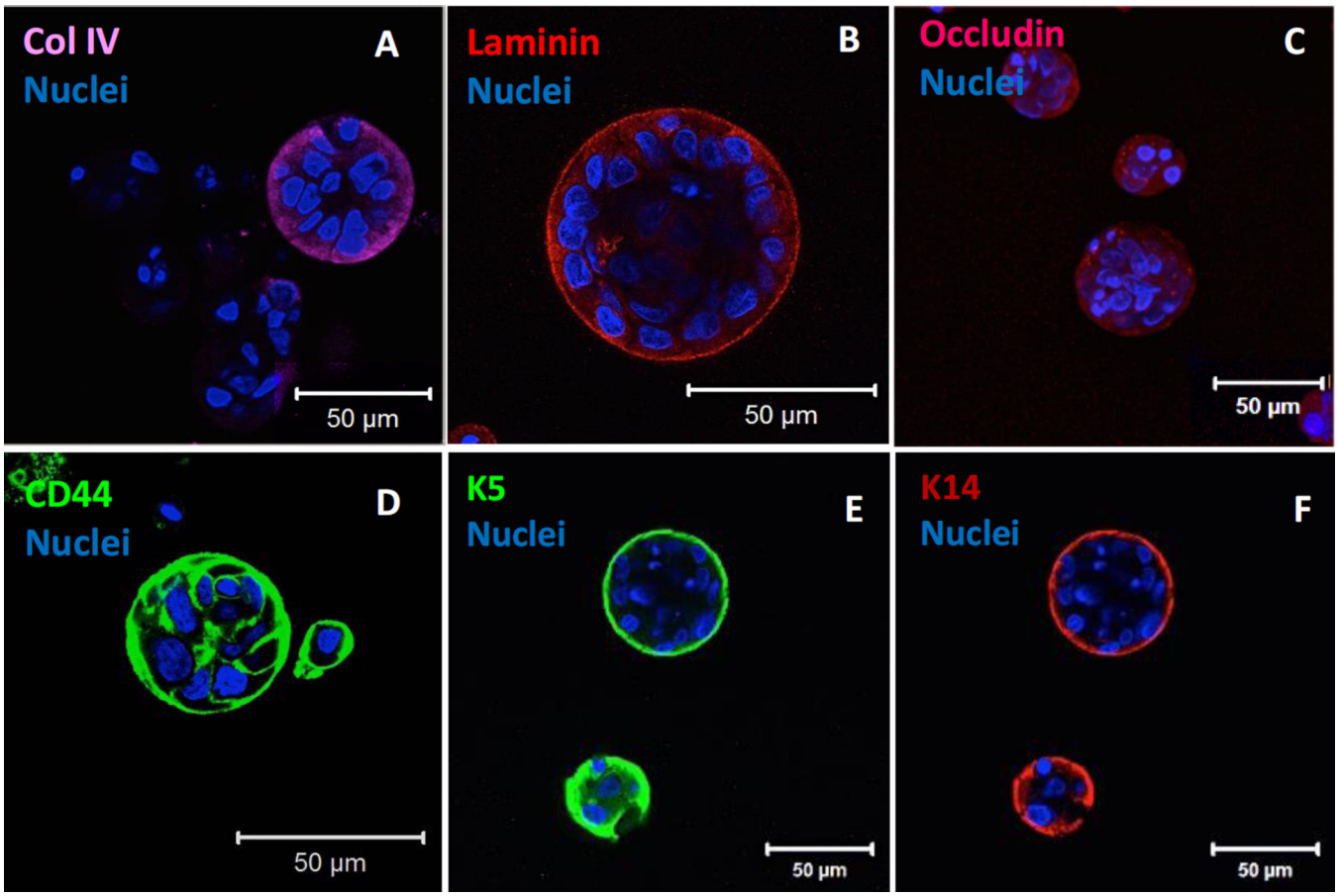

Figure 8.

Immunofluorescence characterization of protein expression by hS/PCs grown in DRC18 gels for 28 days. Cells cultured under these conditions deposited important membrane proteins, such as collagen IV (A, purple) and laminin (B, red), formed tight cell-cell junctions as stained by occludin (C, red) and expressed stem/progenitor markers CD44 (D, green), K5 (E, green), K14 (F, red). Cell nuclei was counter stained as blue and red by using DAPI.

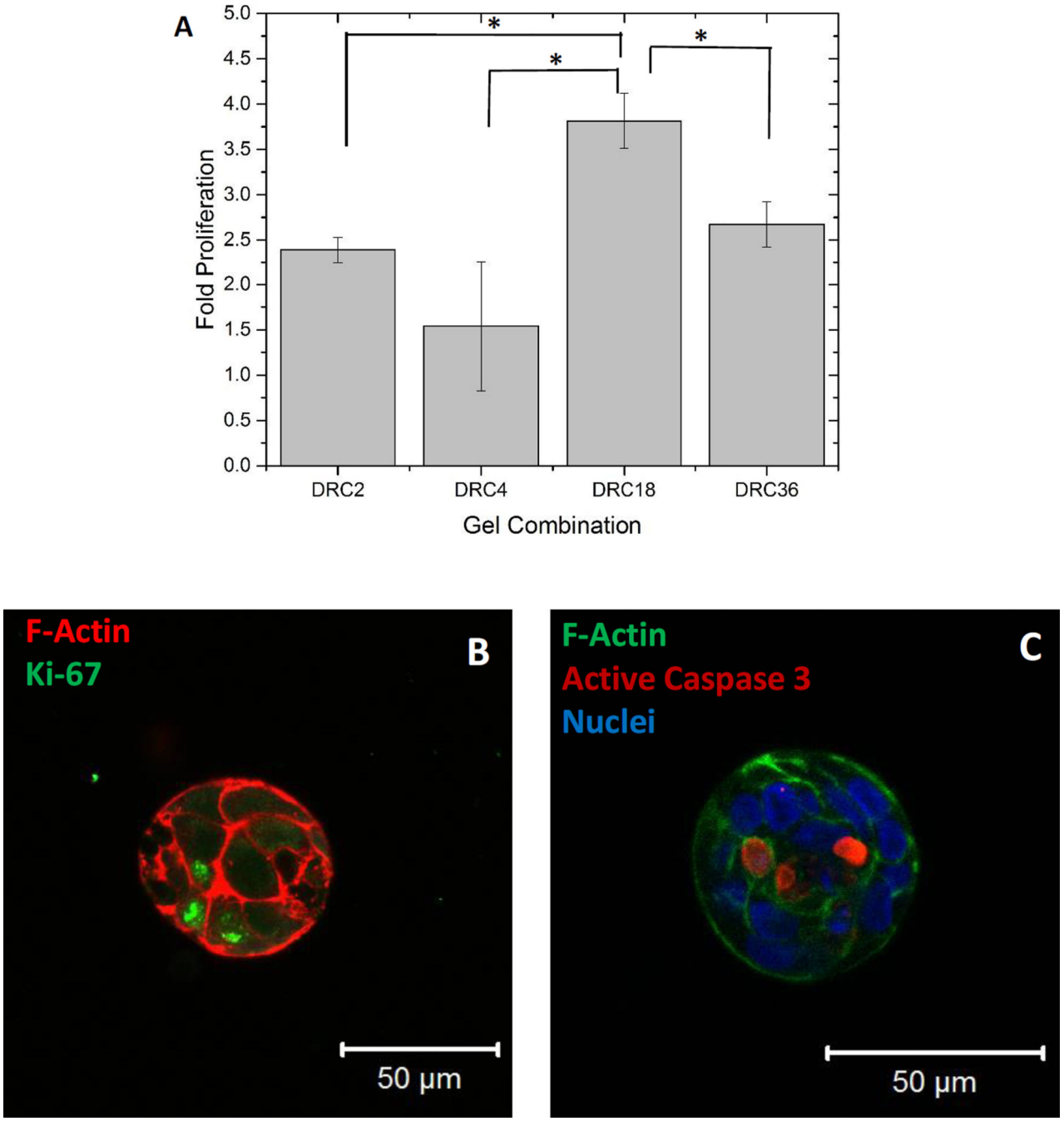

Figure 9.

Differential proliferation and apoptosis of hS/PCs grown in HA hydrogels. (A). Proliferation of hS/PCs in DRC2, DRC4, DRC18 and DRC36 gels as quantified by PicoGreen DNA assay. The fold change in proliferation was calculated by normalizing the cell number at day 28 to that at day 0. The initial seeding density was 1×10^6 cells/mL (*: significant difference, $p<0.05$). (B). Proliferation of hS/PCs cultured in DRC18 gels assessed by Ki67 (green) immunofluorescence staining (Nuclei: blue, F-actin: red). (C): Cellular apoptosis revealed

by positive caspase 3 (red) staining. Cell nuclei and cortical F-actin was stained blue and green, respectively.

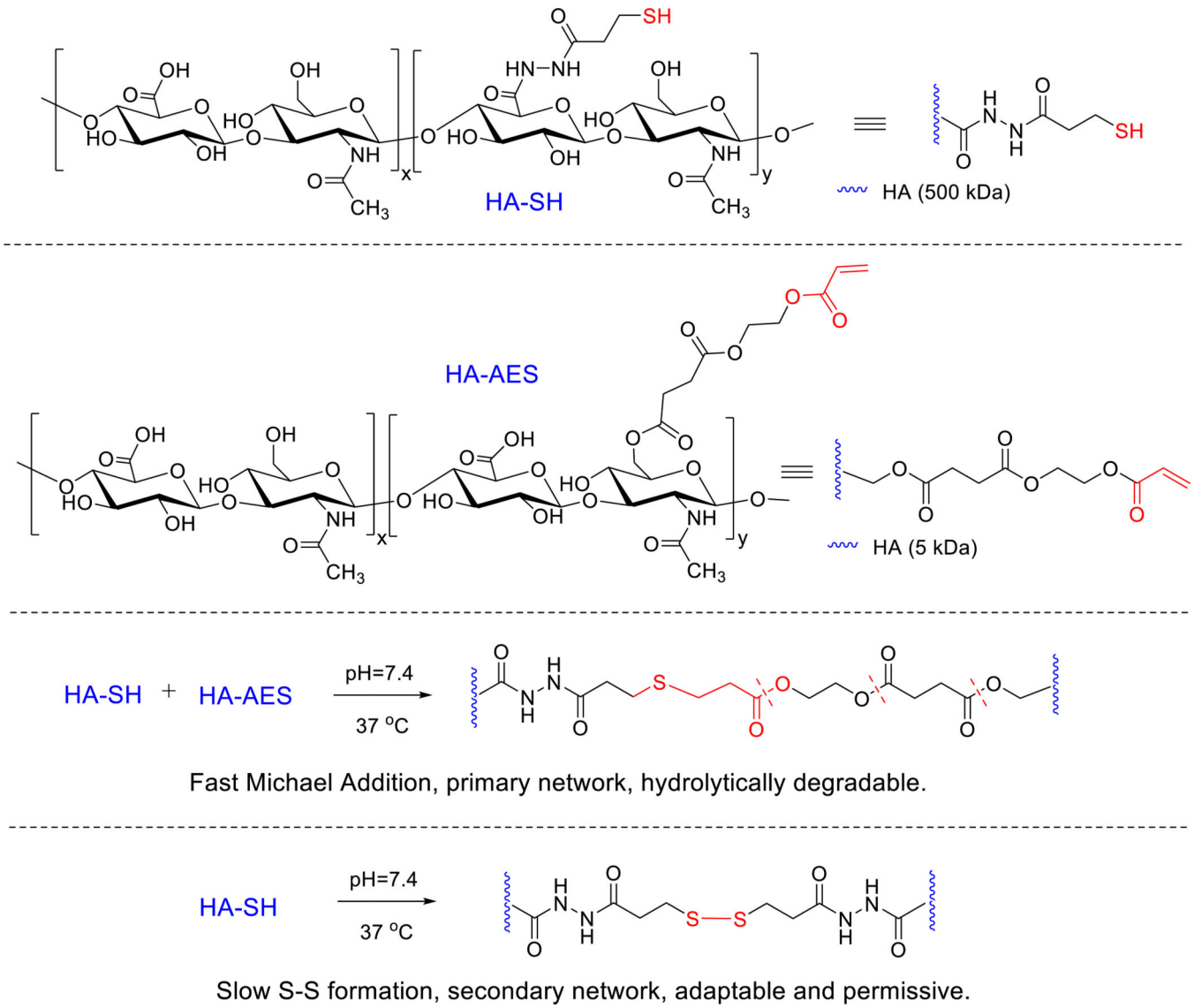

Scheme 1.

Synthesis of HA-based hydrogels via the covalent crosslinking of HA-AES and HA-SH. Fast thiol/acrylate Michael reaction contributes to the establishment of the primary network that is hydrolytically degradable. The disulfide crosslinks, formed gradually and spontaneously, stabilize the primary network, at the same time, introducing adaptable and dynamic features to the network to facilitate the 3D assembly of hS/PCs.

Table 1

Summary of hydrogel formulations investigated for the 3D culture of hS/PCs.

ID	Stock Solution		Hydrogel				
	HA-SH (mg/mL)	HA-AES (mg/mL)	[SH]/[AES] (mol/mol)[a]	HA Conc. (wt %)	G' (Pa)[b]	G" (Pa)[c]	t_{10} (min)[d]
DRC2	10	100	1.8/1.0	1.43	808 ± 159	1.4 ± 0.4	6.3 ± 2.4
DRC4	20	100	3.6/1.0	2.38	1897 ± 81	4.4 ± 0.3	5.6 ± 3.3
DRC18	10	10	18.2/1.0	1.00	35 ± 2	0.3 ± 0.1	14.9 ± 3.8
DRC36	20	10	36.5/1.0	1.95	216 ± 59	3.6 ± 0.9	18.3 ± 5.7

[a] Hydrogels were prepared by mixing the respective stock solutions at the same volume ratio of 20/1 (HA-SH/HA-AES).

[b] Average storage modulus 2 h after the hydrogel precursors were mixed.

[c] Average loss modulus 2 h after the hydrogel precursors were mixed.

[d] Time required for G'=10×G", indicating the establishment of a self-support viscoelastic solid.

ACS Biomater Sci Eng. Author manuscript; available in PMC 2016 December 14.